BIOCHEMISTRY
including biophysical chemistry & molecular biology
Article

Biochemistry **2010,** *49,* 10357–10370 10357
DOI: 10.1021/bi101518x

Unique Properties of the Mtr4p−Poly(A) Complex Suggest a Role in Substrate Targeting†

Jade Bernstein,‡ Jeff D. Ballin,‡ Dimeka N. Patterson,‡ Gerald M. Wilson,‡,§ and Eric A. Toth*,‡,§

‡*Department of Biochemistry and Molecular Biology and* §*Marlene and Stewart Greenebaum Cancer Center, University of Maryland School of Medicine, Baltimore, Maryland 21201, United States*

Received September 17, 2010; Revised Manuscript Received November 3, 2010

ABSTRACT: Mtr4p is a DEVH-box helicase required for 3′-end processing and degradation of various nuclear RNA substrates. In particular, Mtr4p is essential for the creation of 5.8S rRNA, U4 snRNA, and some snoRNAs and for the degradation of cryptic unstable transcripts (CUTs), aberrant mRNAs, and aberrant tRNAs. Many instances of 3′-end processing require limited polyadenylation to proceed. While polyadenylation can signal degradation in species from bacteria to humans, the mechanism whereby polyadenylated substrates are delivered to the degradation machinery is unknown. Our previous work has shown that Mtr4p preferentially binds poly(A) RNA. We suspect that this preference aids in targeting polyadenylated RNAs to the exosome. In these studies, we have investigated the mechanism underlying the preference of Mtr4p for poly(A) substrates as a means of understanding how Mtr4p might facilitate targeting. Our analysis has revealed that recognition of poly(A) substrates involves sequence-specific changes in the architecture of Mtr4p−RNA complexes. Furthermore, these differences significantly affect downstream activities. In particular, homopolymeric stretches like poly(A) ineffectively stimulate the ATPase activity of Mtr4p and suppress the rate of dissociation of the Mtr4p−RNA complex. These findings indicate that the Mtr4p−poly(A) complex is unique and ideally suited for targeting key substrates to the exosome.

Quality control of nuclear RNA requires both processing and surveillance pathways. In particular, ribosomal (rRNA),[1] small nucleolar (snoRNA), small nuclear (snRNA), and messenger (mRNA) RNAs are all transcribed as precursor RNAs (pre-RNAs) that must then be cleaved and/or trimmed to produce functional RNAs (*1*). Any byproducts from the conversion of pre-RNA to functional RNA must be rapidly degraded. Likewise, many aberrant RNAs are subjected to surveillance and thereby eliminated from the nuclear RNA pool to maintain proper cell function. The nuclear exosome is the major degradation machine involved in both pathways of nuclear RNA quality control. In *Saccharomyces cerevisiae*, the nuclear exosome is a collection of six RNase PH homologues (Rrp41p, Rrp42p, Rrp43p, Rrp45p, Rrp46p, and Mtr3p) that are inactive and form a scaffolding ring structure (*2*), three putative RNA binding proteins (Rrp4p, Rrp40p, and Csl4p) that form a cap on the RNase PH hexamer (*3*), and two active 3′ → 5′ exonucleases, Rrp44p (*2*−*4*) and Rrp6p (*5*, *6*). Rrp44p also possesses an endonuclease domain that is important for exosome function. Many exosome substrates contain structured segments that preclude complete processing or degradation by the exosome alone, thus requiring cofactors to ensure the generation of the desired end product. One of those cofactors, Mtr4p, is an indispensible partner of the exosome and is likely responsible for maintaining the momentum of exonucleolytic activity as both Mtr4p and the exosome move through structured regions of some RNA substrates. Mtr4p has been linked to the processing of a diverse population of pre-RNAs. In conjunction with the exosome, Mtr4p assists in processing the 7S rRNA precursor to produce 5.8S rRNA, an essential component of the 60S ribosomal subunit (*7*). Mtr4p is also required for processing some snRNAs and snoRNAs (*8*). Specifically, Mtr4p is involved in the 3′ end maturation of U4 snRNA, a part of the U4/U5·U6 trimer that is recruited during spliceosome assembly (*7*). In addition to its processing function, Mtr4p participates in the nuclear surveillance pathway that degrades aberrant RNAs. Mtr4p helps degrade aberrant mRNAs such as those modified by inappropriate adenylation, splicing, or other abnormalities (*9*, *10*). Some of the surveillance activities of Mtr4p are performed in the context of the TRAMP (Trf−Air−Mtr4 polyadenylation) complex. TRAMP is a three-protein complex consisting of Mtr4p, a poly(A) polymerase (Trf4p or Trf5p), and a zinc-knuckle protein (Air1p or Air2p) (*11*, *12*). As part of the TRAMP complex, Mtr4p participates in both rRNA and snoRNA surveillance (*9*, *13*, *14*). Mtr4p also assists in TRAMP-assisted degradation of hypomodified $tRNA_i^{Met}$ (*12*, *15*, *16*) and cryptic unstable transcript RNAs (CUTs) (*12*, *15*−*18*).

Mtr4p belongs to the Ski2-like family of DExH- and DExD-box helicases within superfamily 2 and possesses both RNA-dependent ATPase activity and ATP-dependent 3′ → 5′ RNA helicase activity (*16*, *19*). Genetics experiments have shown that depletion of Mtr4p in cells is lethal and that the helicase motifs of Mtr4p are critical for its function in vivo. In particular, mutations of the conserved lysine in motif I (Lys-177) or of the conserved serine of motif III (Ser-293) result in dominant negative growth defects (*20*). Recent crystal structures of apo Mtr4p (*21*) and an

†This work was supported funds from the Marlene and Stewart Greenebaum Cancer Center (E.A.T.) and National Institutes of Health Grant R01 CA102428 (G.M.W.).

*To whom correspondence should be addressed: Department of Biochemistry and Molecular Biology, University of Maryland School of Medicine, 108 N. Greene St., Baltimore, MD 21201. Telephone: (410) 706-5345. Fax: (410) 706-8297. E-mail: etoth001@umaryland.edu.

[1]Abbreviations: Fl, fluorescein; EMSA, electrophoretic mobility shift assay; ss, single-stranded; ds, double-stranded; nt, nucleotide; AMP-PNP, adenosine 5′-(β,γ-imido)triphosphate; rRNA, ribosomal RNA; mRNA, messenger RNA; tRNA, transfer RNA; CUT, cryptic unstable transcript.

Published on Web 11/08/2010

Mtr4p−ADP−RNA (*22*) complex reveal that the canonical recA-like core domains are decorated with both winged-helix and seven-helix bundle domains similar to those found in the related archaeal Hel308 helicase (*23*) and a novel arch domain. The arch domain is both unique to the Ski2-like helicases and essential for Mtr4p function (*21*). Such unique sequence and structural features of Mtr4p and related helicases likely contribute to attributes that differentiate them from other enzymes in the same superfamily. One remarkable feature of Mtr4p is its distinct preference for binding short poly(A) tracts (*19*). While previous studies identified this preference, the factors that control selective binding to poly(A) substrates are not well-understood. Further, the parameters that define a stable Mtr4p−RNA complex as a function of RNA sequence have yet to be determined. Finally, the extent to which sequence-specific interactions affect downstream activities such as ATPase activity is unclear. Thus, we undertook a series of experiments to quantitatively assess the impact of RNA substrate sequence on the affinity and stability of Mtr4p−RNA complexes and the efficiency with which Mtr4p hydrolyzes ATP.

The ability of Mtr4p to recognize free 3′-poly(A) tails generated by TRAMP-mediated polyadenylation is a prerequisite for exosome-mediated cleavage of those substrates, as depletion of Mtr4p in vivo gives rise to extended polyadenylated forms of a variety of nuclear RNAs (*7*, *8*, *24*). Thus, understanding the mechanism whereby Mtr4p recognizes poly(A) RNA is key to understanding how Mtr4p promotes processing of TRAMP substrates by the exosome. It is possible that such recognition leads directly to Mtr4p-mediated recruitment of the exosome for processing. The ability of Mtr4p to both remodel structured RNA and target polyadenylated substrates to the exosome would be advantageous for promoting the processing and degradation of highly structured substrates.

In this study, we report that both the substrate sequence and the nucleotide-bound state have a striking effect on the biochemical properties of Mtr4p−RNA complexes. In particular, we show Mtr4p binds poly(A) via a novel mechanism that generates a different architecture for the Mtr4p−poly(A) complex than for other complexes. We also show that poly(A) suppresses both ATPase activity and complex dissociation relative to the random-sequence substrate. Taken together, our data show that the Mtr4p−poly(A) interaction is uniquely configured to promote targeting. Further, some unique properties of the Mtr4p−poly(A) interaction exist independent of ATPase activity, indicating that one role of Mtr4p is to discriminate between substrates and thereby maintain contact with the short polyadenylated sequences that signal degradation.

EXPERIMENTAL PROCEDURES

Cloning, Expression, and Purification of Full-Length S. cerevisiae Mtr4p. Recombinant *S. cerevisiae* Mtr4p was expressed and purified as previously described (*19*). We evaluated the homogeneity of the protein in solution (typical particle size of ~12 nm) using dynamic light scattering in a Zetasizer Nano S (Malvern Instruments). Recombinant Mtr4p was snap-frozen and stored at −80 °C.

RNA Substrates. Synthesis, 2′-hydroxyl deprotection, and purification of the RNA substrates (listed in Table 1) used in this study were performed by Dharmacon Research or Integrated DNA Technologies. Fluorescein groups were linked to the 5′-ends of some of the RNA substrates during solid-phase synthesis and are designated by the prefix "Fl" where applicable. Lyophilized RNA samples were resuspended in 1× TE buffer. RNA yields were quantified by absorbance spectroscopy at OD_{260} in a Beckman DU-640 spectrophotometer and the ε_{260} of each substrate, provided by the manufacturer. Fluorophore labeling efficiencies were quantified by absorbance, incorporating fractional contributions of coupled fluorophores to OD_{260} for substrates containing fluorescein (Fl) moieties as previously described (*25*).

Table 1: RNA Substrates Used in This Study

RNA substrate	sequence (5′ → 3′)
R_{20}	(Fl)UGUCAUAAAUAUGUAUUCAA
A_{20}	(Fl)AAAAAAAAAAAAAAAAAAAA
U_{20}	(Fl)UUUUUUUUUUUUUUUUUUUU
$(UC)_{10}$	(Fl)UCUCUCUCUCUCUCUCUC
A_{10}	(Fl)AAAAAAAAAA
A_5	(Fl)AAAAA
R_{10}	(Fl)UGACGCGAGA
R_5	(Fl)UGUCA

Table 2: Binding Density Analysis of A_{20} and R_{20} Substrates in Various Nucleotide-Bound States

substrate	nucleotide	intersection site size (bases)
A_{20}	none	5.3 ± 0.8
A_{20}	AMP-PNP	4.9 ± 0.9
A_{20}	ADP	4.8 ± 0.5
R_{20}	none	5.3 ± 1.0
R_{20}	AMP-PNP	16.7 ± 2.9
R_{20}	ADP	6.8 ± 1.9

These four different 20-nucleotide RNA sequences were chosen for their similarity to potential in vivo substrates and their limited propensity to form higher-order structures. The substrate length (20 nt) reflects the average number of adenylates added by the Trf4p polymerase of the TRAMP complex to hypomethylated pre-$tRNA_i^{Met}$ in vivo (*15*). One substrate is a purine homopolymer (A_{20}). The addition of a poly(A) tail is a known degradation signal for RNAs within the nucleus (*11*, *12*). Poly(A) substrates can form a single helix in solution (*26*) but when interacting with poly(A)-binding proteins generally show an extended poly(A) structure (*27*, *28*). The second substrate contains a random sequence (R_{20}) and was designed to represent general RNA. Specifically, the R_{20} substrate was designed to lack both repetitive sequences and significant secondary structure [as determined by RNA structure prediction programs (*29*, *30*)]. The third substrate, a pyrimidine homopolymer (U_{20}), was used to control for effects that are due to the presence of a homopolymer and are not specific to poly(A). At low temperatures, poly(U) substrates can fold to form hairpins that result in double-helical structures (*31*). To evaluate potential consequences of the U_{20} substrate forming higher-order structures as a factor in our results, we inserted alternating cytosines in the U_{20} substrate that are expected to eliminate any propensity to form such structures, thereby creating the fourth substrate [$(UC)_{10}$].

Mtr4p Binding Density Analysis. The average size of the Mtr4p binding site to the RNA substrates A_{20} and R_{20} (Table 2) was determined as a function of nucleotide-bound state using the model-independent Macromolecular Competition Titration Method (MCT) of Jezewska and Bujalowski (*32*, *33*). This quantitative approach determines the free protein concentration (P_F) and binding density ($\Sigma\nu$) for isotherms describing association of a ligand (i.e., Mtr4p, in this study) with a macromolecule

[i.e., fluorescein-labeled RNA (Fl-RNA)]. We define binding density as the average number of Mtr4p proteins bound per strand of Fl-RNA. These thermodynamic parameters were extracted from analysis of a series of Mtr4p protein titrations against at least three different RNA concentrations. The total RNA population consisted of 1 nM Fl-RNA supplemented with increasing amounts of equivalent sequence but nonfluorescent RNA competitor (typically final RNA concentrations of 5−45 nM) to generate binding isotherms that were shifted to higher protein concentrations. The anisotropy measurements were conducted using a Beacon 2000 Variable Temperature Fluorescence Polarization System equipped with fluorescein excitation (485 nm) and emission (535 nm) filters. A typical reaction mixture (100 μL) contained a limiting concentration (1 nM) of an Fl-RNA substrate, binding buffer [10 mM Tris-HCl (pH 8), 40 mM NaCl, 2 mM dithiothreitol, 1 mM adenosine 5′-(β,γ-imido)triphosphate (AMP-PNP) or ADP, and 5 mM $MgCl_2$ when indicated], and an increasing concentration of protein (0−2.5 μM). In addition, a second set of reaction conditions was used to aid in determining the effects of salt concentrations closer to the physiological range on the reaction. The buffer system for those experiments contained 5 mM Tris-HCl (pH 8), 2 mM dithiothreitol, 90 mM potassium acetate, and 1 mM magnesium acetate (*34*−*37*). The polarimeter was operated in static mode using a single sample containing all components, except the labeled RNA and protein, which was read as a blank before the experiment began. Samples were incubated following addition of the labeled RNA until they reached equilibrium before anisotropy was measured. The equilibration time was determined by the dissociation kinetics measurements to be either 1 min for R_{20} or 30 min for A_{20}. Mtr4p−RNA binding was monitored by the net change in fluorescence anisotropy ($\Delta A_{obs} = A_x - A_0$, where A_x is the observed anisotropy in the presence of x nM Mtr4p and A_0 is the anisotropy in the absence of protein). Because ΔA_{obs} is exclusively determined from the extent of ligand (Mtr4p) binding to the Fl-RNA, all curves span the same anisotropy range and plateau to the same maximum value at saturation. The isotherms shift to the right in the presence of an increased nonfluorescent RNA competitor concentration (R_C) because more protein is necessary to saturate the competing lattice. ΔA_{obs} reflects the population-weighted average of contributions from all Mtr4p−Fl-RNA complexes, each with its own intrinsic anisotropy contribution ΔA_j for the jth species. Because ΔA_{obs} is correlated to a unique distribution of Mtr4p−Fl-RNA complexes, a pair of RNA competitor and total protein concentrations (R_{C_1} and P_{T_1}) obtained from one isotherm at a given ΔA_{obs} has the same P_F and $\Sigma\nu_R$ values as the concentration pair (R_{C_1} and P_{T_2}) that possesses the same ΔA_{obs} in a second isotherm. $\Sigma\nu_R$ denotes the binding density of Mtr4p with Fl-RNA, where R indicates reference. By conservation of mass, for any two total protein concentrations P_{T_1} and P_{T_2} that have equal ΔA_{obs} values upon titration against unlabeled RNA concentrations R_{C_1} and R_{C_2} in the presence of a common concentration of labeled RNA (e.g., R_R = 1 nM)

$$P_{T_1} = (\Sigma\nu_R)R_{T_R} + (\Sigma\nu_C)R_{C_1} + P_F \quad (1)$$

$$P_{T_2} = (\Sigma\nu_R)R_{T_R} + (\Sigma\nu_C)R_{C_2} + P_F \quad (2)$$

By subtracting eq 2 from eq 1, we can obtain the binding density to the unlabeled RNA:

$$\Sigma\nu_C = \frac{P_{T_2} - P_{T_1}}{R_{C_2} - R_{C_1}} \quad (3)$$

and the free protein concentration is calculated by

$$P_F = P_{T_i} - (\Sigma\nu_R)R_{T_R} - (\Sigma\nu_C)R_{C_i} \quad (4)$$

where i = 1 or 2, denoting the specified protein concentrations P_{T_1} versus P_{T_2} or R_{T_1} versus R_{C_2}. This analysis requires no prior knowledge of the binding mechanism and makes no assumptions about the relative binding affinity of Mtr4p for Fl-RNA or competitor RNA (i.e., the analysis is applicable regardless of whether $\Sigma\nu_R$ and $\Sigma\nu_C$ are the same or different). In any case, plotting the anisotropy change, ΔA_{obs}, as a function of $\Sigma\nu_C$ allows one to obtain the binding stoichiometry of the Mtr4p−nonfluorescent RNA complex (Figure 1). The correlation of $\Sigma\nu_R$ with ΔA_{obs} and with P_F in the absence of competitor can be determined by Macromolecular Binding Density Analysis (MBDA) (*33*, *38*) of analogous protein titrations against a series of Fl-RNA concentrations (with no unlabeled competitor). Given $\Sigma\nu_C$ derived from MCT analysis and using the ΔA_{obs} to calculate $\Sigma\nu_R$ using the relationship obtained from MBDA, the unbound protein concentration P_F is obtained from eq 4 and can be independently validated by comparison to the P_F found from MBDA. In this way, the free protein concentration, as well as the population-averaged binding densities of unlabeled RNA ($\Sigma\nu_C$) and Fl-RNA ($\Sigma\nu_R$), can be calculated without approximation or any assumptions about the binding mechanism.

RNA Binding. RNA binding affinity was measured using a fluorescence anisotropy-based assay according to the method of Brewer and colleagues (*25*, *39*). The anisotropy measurements were conducted under the same solution conditions that are described for MBDA above. A typical reaction mixture (100 μL) contained a limiting concentration (0.2 nM) of an RNA substrate labeled with fluorescein at its 5′-end, binding buffer (with 1 mM AMP-PNP or ADP and 5 mM $MgCl_2$, when indicated), and an increasing concentration of protein (0−2.5 μM). The equilibration time was determined by the dissociation kinetics measurements to be either 30 min for A_{20} and A_{10} substrates or 1 min (all other substrates). The total intensity of emission was monitored concurrent with anisotropy to ensure that interactions between Mtr4p and the RNA substrate did not affect the quantum yield of the fluorophore. In cases in which the total fluorescence emission varied as a function of added protein concentration, an appropriate correction factor (*40*−*42*) was applied to the measured anisotropies. Single-site equilibrium association constants were calculated from the binding data using GraphPad Prism version 3.03 and eq 5 (*25*):

$$A_{total} = \frac{A_{RNA} + A_{complex}K_a[P]}{1 + K_a[P]} \quad (5)$$

where A_{total} represents the total anisotropy, A_{RNA} is the intrinsic anisotropy of the RNA in the absence of protein, $A_{complex}$ is the anisotropy of the saturated protein−RNA complex, [P] is the protein concentration, and K_a is the association constant. This binding model assumes that one binding site (or multiple equivalent binding sites) exists on the substrate RNA. The appropriateness of the single-binding site model was evaluated by the agreement between the observed and calculated binding isotherms and the random distribution of residuals. In cases in which the single-site model was deemed inappropriate, binding isotherms were analyzed using a variant of the Hill equation (*43*):

$$A_{total} = A_{comp} + (A_{comp} - A_{RNA})\left[\frac{([P]/[P]_{1/2})^h}{1 + ([P]/[P]_{1/2})^h}\right] \quad (6)$$

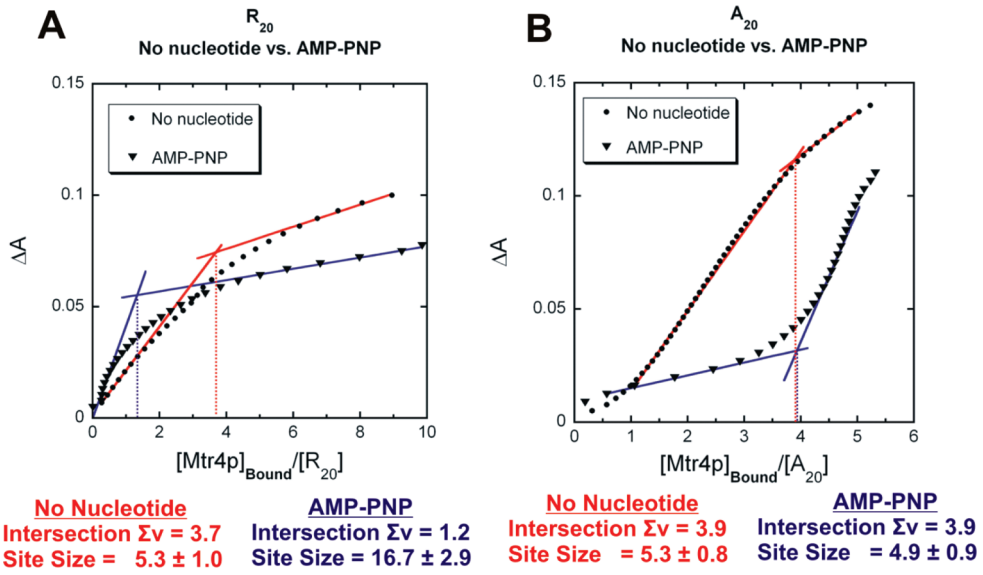

FIGURE 1: Binding density analysis of Mtr4p binding to R_{20} and A_{20} identifies major differences in complex architecture. The Mtr4p-dependent change in the fluorescence anisotropy (ΔA) of fluorescein-labeled ssRNA substrates (Table 1) was calculated as a function of the average number of Mtr4p molecules bound per RNA strand (Σv) as described in Experimental Procedures. The solid lines are tangent to slopes corresponding to the low- and high-binding density modes of the isotherms. The dotted lines represent the intersections of the two phases, which is taken as the stoichiometry of the larger site size binding mode (values indicated below each plot). (A) Analysis of the R_{20} substrate in the absence of nucleotide (red lines) and in the presence of AMP-PNP (blue lines). (B) Analysis of the A_{20} substrate in the absence of nucleotide (red lines) and in the presence of AMP-PNP (blue lines).

where A_{total} is the measured anisotropy, A_{comp} is the anisotropy of the saturated protein−RNA complex, A_{RNA} is the inherent anisotropy of the RNA substrate, and h is the Hill coefficient. This equation returns an estimate of the amount of protein required to achieve half-maximal signal intensity ($[P]_{1/2}$) that, in the case of a single binding site (i.e., $h = 1.0$), is equivalent to the K_d.

Enzyme Kinetics. A coupled pyruvate kinase−lactate dehydrogenase assay was used to assess the Michaelis−Menten kinetics of ATPase activity as described previously (*44*) with minor modifications. Briefly, Mtr4p (100 nM) was incubated with varying concentrations of ATP (0−5 mM) and either 500 nM RNA or 1 μM RNA, depending on the K_m of the particular RNA, at 37 °C. A typical reaction mixture (0.5 mL) contained 50 mM sodium HEPES (pH 7.5), 50 mM NaCl, 5 mM $MgCl_2$, 0.1 mM EDTA, 1 mM dithiothreitol, 0.2 mM NADH, 1 mM phosphoenolpyruvate, 3.5 units of pyruvate kinase, and 5 units of lactate dehydrogenase. In a parallel experiment, Mtr4p was incubated with varying amounts of RNA (0−4 μM) and 4 mM ATP under the same conditions that are described above. Oxidation of NADH to NAD^+, which is coupled to ATP hydrolysis, was continuously monitored at 338 nm in a Beckman DU-640 spectrophotometer. Initial rates were calculated from the change in absorbance using a net extinction coefficient ($\Delta\varepsilon_{338}$) of $-6220\ M^{-1}\ cm^{-1}$ (reflecting the fact that the conversion of NADH to NAD^+ decreases absorbance at 338 nm). As a control, the absorbance change as a function of time for samples without ATP or RNA, depending on the experiment, was subtracted from the initial rate at each ATP or RNA concentration. Kinetic parameters were determined by fitting the rates as a function of ATP or RNA concentration to the Michaelis−Menten equation using KaleidaGraph (Synergy Software). The lack of detectable ATP hydrolysis in the presence of R_{20} for either of two ATPase-deficient Mtr4p mutants (K177A and D262A) confirms that contaminating ATPases do not interfere with these experiments (data not shown).

RNA−Protein Complex Dissociation Kinetics. To determine the kinetic parameters for release of each of the four Mtr4p 20 nt substrate complexes (Table 1), we incubated a fixed amount of protein (150 nM) with fluorescein-labeled ssRNA and measured the decrease in anisotropy as a function of time. Dissociation of the Mtr4p−RNA complex was stimulated by a competitive challenge with a 5000-fold molar excess of unlabeled ssRNA of the same sequence. The solution conditions were identical to those employed in the binding affinity experiments. The polarimeter was operated in kinetic mode using a single sample containing all components except the RNAs as a blank. At the initial time point, the sample contained all components, except the unlabeled competitor RNA. The unlabeled ssRNA was then added, and measurements were taken every 15 s for at least 150 s. The total fluorescence emission intensity was monitored concurrently with anisotropy to ensure that photobleaching of the fluorescein did not affect the observations. The total fluorescence intensity at the end of each kinetic trace was typically within 5% of the starting value (not shown). The kinetics of complex dissociation was measured for each of the substrates either in the absence of nucleotide, in the presence of AMP-PNP, or in the presence of ATP. The time-dependent decrease in anisotropy was fit to a single-exponential equation (where appropriate):

$$A = A_0 e^{-kt} + B \quad (7)$$

where A is the measured anisotropy at time t, A_0 is the amplitude of the reaction at the beginning of the dissociation event, k is the rate of complex dissociation, t is time, and B is the minimum anisotropy (i.e., the plateau of the reaction). The initial anisotropy is equal to $A_0 + B$. This model assumes that only one dissociation event is taking place. The appropriateness of the single-exponential model was evaluated by the agreement between the observed and calculated kinetic traces as determined by a residual runs test. In cases in which the single-exponential equation was deemed inappropriate, isotherms were analyzed by a two-component exponential equation:

$$A = A_0 e^{-k_1 t} + A_1 e^{-k_2 t} + B \quad (8)$$

where A is the measured anisotropy at time t, A_0 is the amplitude of the fast phase of dissociation, A_1 is the estimated amplitude of the slow phase of dissociation, k_1 is the rate of the faster dissociation event, k_2 is the rate of the slower dissociation event, t is the time, and B is the minimum anisotropy. The initial anisotropy is equal to $A_0 + A_1 + B$.

RESULTS

Binding Density Analysis of Mtr4p−RNA Complexes Reveals Substrate-Specific Changes to Complex Architecture. Mtr4p binds RNA with a clear preference for short poly(A) tracts (*19*). However, the basis for this preference is not well-understood. Polyadenylation via the TRAMP complex is a necessary signal that promotes exosome-mediated RNA processing. Thus, understanding the properties that give rise to preferential binding to poly(A) will shed light on how key substrates are selected and targeted for processing by the exosome. We employed MBDA to examine the differences between Mtr4p−RNA complexes more explicitly. The change in Mtr4p binding density ($\Sigma\nu$, or number of proteins bound per RNA) yields important insights into how ATP and sequence-specific RNA interactions affect the Mtr4p−RNA complex architecture and hence how substrates are selected. In addition, the magnitude of observed signal as a function of binding density yields information about the nature of structural changes that accompany complex formation. MBDA can also identify the number of distinct binding modes for a given Mtr4p−RNA complex. The Mtr4p binding density ($\Sigma\nu$) was measured using fluorescence anisotropy in the presence of three different concentrations of RNA for each condition (i.e., A_{20} and R_{20}; nucleotide-free, ADP-bound, and AMP-PNP-bound for both substrates). These three binding isotherms were analyzed by MBDA to assess complex behavior and to determine the number of nucleotides Mtr4p occludes upon binding to a particular substrate in a given nucleotide-bound state. The nonlinear nature of the change in anisotropy as a function of binding density indicates that these Mtr4p titrations exhibit at least two binding modes for both the A_{20} and R_{20} substrates, a low-binding density mode and a high-binding density mode. The stoichiometry of the low-binding density mode was determined as follows. The Mtr4p-dependent change in fluorescence anisotropy (ΔA) was calculated as a function of the average number of Mtr4p molecules bound per RNA strand ($\Sigma\nu$) as described previously (*33*). Tangent lines to slopes corresponding to low- and high-density phases of the isotherm (*45*) were then calculated. The intersection of the two phases was taken as the stoichiometry of the low-binding density mode (*45*). From the stoichiometry and the assumption that there is only one RNA strand bound by a given Mtr4p protein, the site size is simply calculated as ($N/\Sigma\nu_i$), where N is the number of nucleotides in the substrate and $\Sigma\nu_i$ is the binding density for complex i. Saturation of RNA with Mtr4p requires very high protein concentrations and varies little with substrate or nucleotide. Therefore, we focused on the low-binding density mode to determine thermodynamic differences between substrates and the nucleotide-bound state.

For the Mtr4p−R_{20} complex, the site size of the low-binding density mode increased markedly as a function of nucleotide-bound state: from 5.3 ± 1.0 nt in the nucleotide-free complex, to 6.8 ± 1.9 nt in the ADP-bound complex, and finally to 16.7 ± 2.9 nt in the AMP-PNP-bound complex (Table 2). However, the overall architecture of the complex, as judged from the curvature of the ΔA versus $\Sigma\nu_i$ plots (Figure 1A), does not appear to change significantly. The Mtr4p−R_{20} complex exhibits a steep anisotropy dependence on $\Sigma\nu$ for the low-binding density mode and a more modest increase for the high-binding density mode, regardless of nucleotide-bound state. This suggests that the primary difference between the nucleotide-free and AMP-PNP-bound complexes is an expansion of the contact surface of RNA occluded by Mtr4p.

In contrast, the site size of the Mtr4p−A_{20} complex in the low-binding density mode does not vary appreciably from 5 nt, regardless of nucleotide-bound state (Table 2). The architecture of the Mtr4p−A_{20} complex, however, appears to change radically upon binding AMP-PNP. This is evident from the dependence of the change in anisotropy on binding density for the Mtr4p−A_{20} versus Mtr4p−A_{20}−AMP-PNP complexes (Figure 1B). For the Mtr4p−A_{20} complex in the low-binding density mode, the change in anisotropy with increasing binding density is steep, which is expected for a complex between a 123 kDa protein (Mtr4p) and a 6 kDa substrate (A_{20}). The increase in anisotropy with increasing binding density is comparatively modest in the high-binding density mode. Strikingly, for the Mtr4p−A_{20}−AMP-PNP complex in the low-binding density mode, a shallow increase in anisotropy is observed. After the transition to the high-binding density mode occurs, the anisotropy increases sharply. The steep slope of the high-binding density mode of the Mtr4p−A_{20}−AMP-PNP complex suggests that this complex undergoes significant conformational remodeling at higher binding densities. Further, on the basis of the behavior of the low-binding density modes, these complexes appear to have distinct architectures at lower binding densities as well.

Presumably, the conformational change in Mtr4p caused by binding of AMP-PNP is similar in the presence of both substrates. Therefore, the ability to induce such different changes in architecture upon binding to either the Mtr4p−R_{20} or Mtr4p−A_{20} complex is noteworthy. These data indicate that conformational changes of the Mtr4p−RNA complex created by binding of ATP are substrate-specific. The distinct binding mode and architecture of the poly(A) complex likely reflect the underlying mechanism via which Mtr4p can distinguish poly(A) from other sequences.

Nucleotide Binding and Substrate Truncation Affect Binding Affinity in a Sequence-Dependent Manner. Changes in binding affinity as a function of RNA sequence, RNA structure, and nucleotide-bound state provide details regarding the conditions that favor targeting to the exosome and Mtr4p-assisted RNA processing. Previous studies clearly showed the following. Mtr4p prefers to bind free 3′-ends; Mtr4p prefers poly(A) substrates to those of random sequences, and nucleotide binding generally decreases the affinity of Mtr4p for RNA substrates (*19*). In these studies, we sought to determine if the trends for poly(A) versus random substrates extended to other repetitive sequences, namely, poly(U) and poly(UC). Thus, we determined the affinity of Mtr4p for the four 20 nt substrates listed in Table 1 by fluorescence anisotropy (Table 3 and ref *19*). From these data, several trends emerge. In particular, Mtr4p exhibits apparent cooperative binding behavior for both the homopolymers (i.e., A_{20} and U_{20}) and the $(UC)_{10}$ repeating sequence. In our previous studies, we observed two bound species in electrophoretic mobility shift assays (EMSAs) for the A_{20} substrate independent of nucleotide-bound status (*19*), and statistical analyses of fits of models to the binding isotherms clearly showed that a single-site model was inappropriate. Despite the

clear presence of two bound species in the EMSA, the two binding events could not be resolved from anisotropy isotherms. Thus, we used a transformed Hill model (eq 6) to fit the observed change in anisotropy as a function of Mtr4p concentration (*19*). With the U_{20} and $(UC)_{10}$ substrates, statistical analyses of model fits also showed that the transformed Hill model was appropriate. A second feature of these binding isotherms is that nucleotide binding modulates the affinity of the Mtr4p−R_{20} complex differently than the other complexes. For the Mtr4p−R_{20} complex, the AMP-PNP-bound species clearly is the lowest-affinity complex. The affinity of Mtr4p for the R_{20} substrate in the presence of ADP was statistically indistinguishable ($p = 0.48$) from that in the absence of nucleotide. In contrast, for the other 20 nt Mtr4p−substrate complexes, the ADP-bound species is the lowest-affinity complex. Other subtle trends are also evident. For the A_{20} and U_{20} substrates, the nucleotide-free species is clearly the highest-affinity complex, whereas for the $(UC)_{10}$ substrate, the AMP-PNP-bound species is the highest-affinity complex. This behavior might reflect the affinity for ATP rather than the $(UC)_{10}$ substrate if the tight binding of RNA in the presence of AMP-PNP reflects a lack of affinity for the nucleotide itself. This idea is supported by the poor Mtr4p ATPase activity when presented with the $(UC)_{10}$ substrate (Table 4 and below). Because differences in solution salt conditions can influence binding properties, we tested the affinity of Mtr4p for both the A_{20} and R_{20} substrates in the absence of nucleotide under near-physiological salt conditions. The univalent salt concentration increase from 50 to 90 mM and the increase from 0 to 1 mM Mg^{2+} significantly weakened the binding to both substrates (data not shown), but the preferential binding of Mtr4p to the A_{20} substrate was maintained under both solution conditions. Thus, we standardized our assay using the lower-ionic strength conditions because the quality of the data is significantly improved over that collected at physiological salt concentrations. In general, for substrates as long as 20 nt, sequence content appears to have an only modest effect on the affinity of Mtr4p for a given substrate. However, both the mode of interaction (i.e., presence of apparent cooperative behavior) and regulation by nucleotide binding differ for random-sequence substrates versus substrates containing repetitive sequences.

Table 3: Comparative Binding Affinities[a] of Mtr4p for Model ssRNA Substrates as a Function of Nucleotide Binding and Length

substrate	no nucleotide	ADP	AMP-PNP
A_{20}	*11 ± 2*[b]	*80 ± 5*[b]	*48 ± 15*[b]
A_{10}	*26 ± 6*	*293 ± 31*[c]	*495 ± 12*[d]
A_5	146 ± 21	> 2000	> 2000
R_{20}	21 ± 4[b]	19 ± 2[b]	89 ± 9[b]
R_{10}	*49 ± 1*	643 ± 63	774 ± 71
R_5	1458 ± 211	> 2000	> 2000[c]
U_{20}	*9 ± 1*	*68 ± 1*	*13 ± 1*
$(UC)_{10}$	*21 ± 1*	*88 ± 6*	*14 ± 2*

[a]Dissociation constant (K_d) = $1/K_a$, averaged over three independent experiments (expressed as the mean value and its standard error), except as indicated by $P_{1/2}$, in which case the half-maximal binding affinity was determined using eqs 5 and 6 (see Experimental Procedures). Values in italics indicate $P_{1/2}$ values instead of K_d values. All values are in nanomolar. Affinities of > 2000 nM were too weak to be determined. [b]Values previously reported (*19*). [c]Represents an average of two replicates, ± the spread of the two measurements, where indicated. [d]Weak binding precluded statistical distinction of using a single-site model vs Hill analysis. The relative affinity is reported as $P_{1/2}$ to facilitate comparison with other A_{10} results.

Sequence content alone is not likely to be the only parameter that affects nucleotide-dependent changes in the affinity of Mtr4p for a given substrate. Substrate length is apt to have a large influence. In the various RNA processing and degradation pathways, Mtr4p acts in concert with the exosome, which truncates substrates by exonucleolytic cleavage. Thus, the ability of Mtr4p to bind shorter ssRNA stretches will significantly impact the ability of Mtr4p to deliver RNAs and assist the exosome in processing substrates containing those sequences at their 3′-end. To examine the ability of Mtr4p to bind short oligonucleotides and to provide an orthogonal examination of Mtr4p site size requirements for comparison with the MBDA described above, we used poly(A) and random-sequence substrates 10 and 5 nucleotides in length (i.e., A_{10}, A_5, R_{10}, and R_5). On the basis of the MBDA analysis, truncating the R_{20} substrate to 10 nucleotides would result in a substrate with two binding sites in the absence of nucleotide, one binding site in the presence of ADP, and fewer than one binding site in the presence of AMP-PNP. For the Mtr4p−poly(A) complexes, truncating the length to 10 nt would remove two binding sites in all nucleotide-bound states. When the R_{20} substrate is reduced to R_{10} in the absence of nucleotide, we observed a 2-fold decrease in affinity. Strikingly, the affinity in the presence of ADP decreases by approximately 33-fold, and the presence of AMP-PNP causes an approximately 12-fold decrease in affinity (Table 3). It is clear that removal of up to two binding sites decreases the affinity of Mtr4p for random-sequence substrates in the absence of nucleotide. For the R_{10}−ADP complex, the loss of binding sites resulting from an increased site size (7 nt) causes a much more profound loss of affinity. Similarly, the Mtr4p−R_{10}−AMP-PNP complex, for which the site size is 17 nt, is a low-affinity complex. It is possible that the presence of bound nucleotide enhances the effect of losing binding sites in the ADP- and AMP-PNP-bound forms. However, the site size of the Mtr4p−R_{20} complex changes significantly upon nucleotide binding, making it difficult to separate the effects of changes in the number of available binding sites from a site size-independent change in affinity caused by nucleotide binding. Reducing the length of the A_{20} substrate to 10 nt did

Table 4: Kinetic Parameters of Mtr4p−ATPase Activity as a Function of Substrate Composition and Length

substrate	k_{cat} (min^{-1})	K_m(ATP) (mM)	k_{max} (min^{-1})	K_{app}(RNA) (nM)	k_{cat}/K_m(ATP) (min^{-1} μM^{-1})
A_{20}	123 ± 18	0.4 ± 0.06	180 ± 13	211 ± 69	308
A_{10}	146 ± 3	5.2 ± 2	182 ± 20	516 ± 77	23
A_5	no activity				
R_{20}	444 ± 17	0.1 ± 0.03	519 ± 42	179 ± 34	4440
R_{10}	163 ± 10	1.1 ± 0.2	163 ± 10	1136 ± 81	148
R_5	101 ± 5	1.2 ± 0.3	48 ± 3.2	1468 ± 578	84
U_{20}	134 ± 11	0.3 ± 0.03	200 ± 56	193 ± 19	447
$(UC)_{10}$	weak	weak	not available	not available	not available

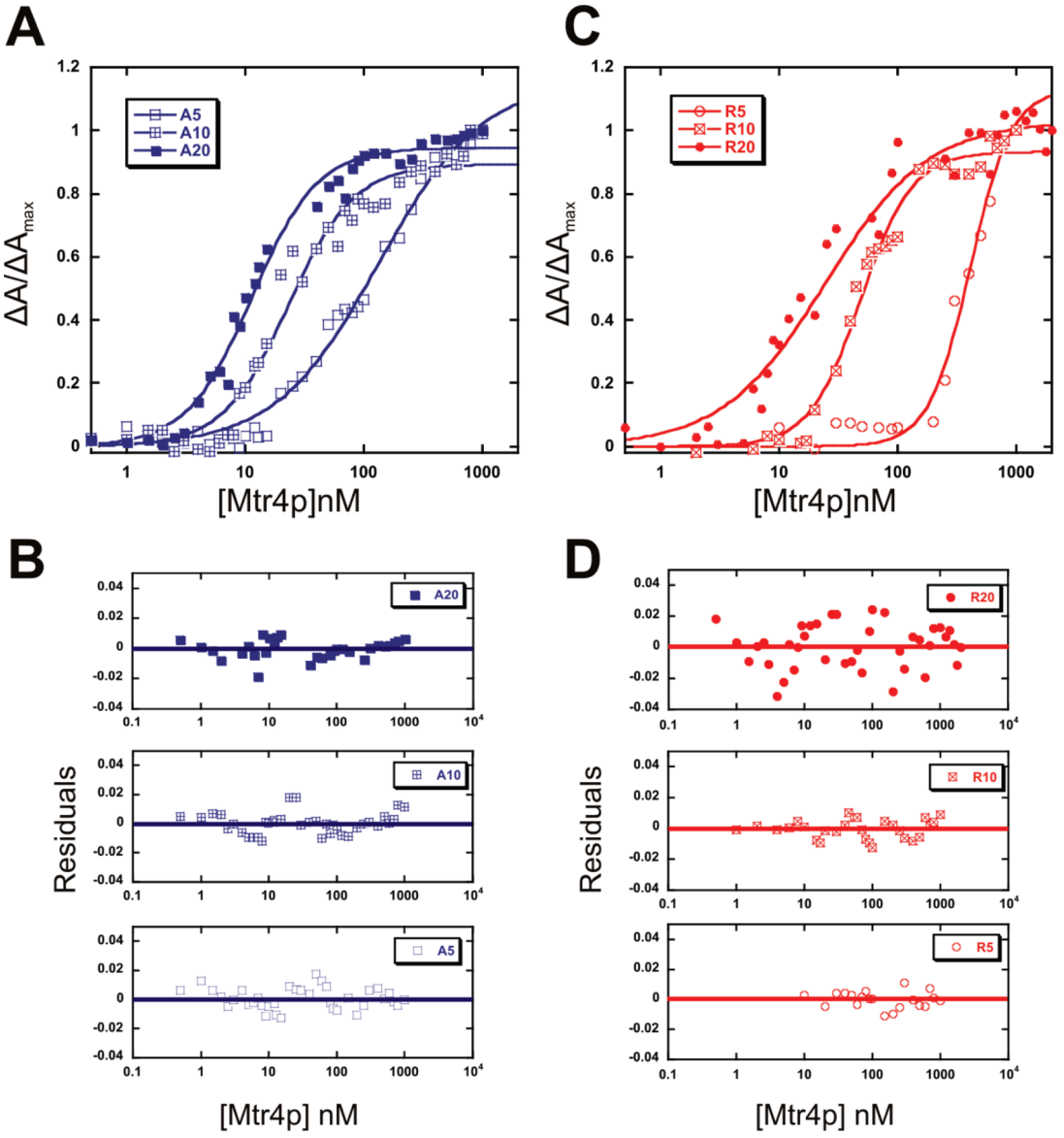

FIGURE 2: Substrate truncation impairs binding of Mtr4p to random-sequence substrates more than poly(A). (A) Representative binding isotherms for the association of Mtr4p with single-stranded 20, 10, and 5 nt poly(A) RNA in the absence of nucleotide (similar trends were observed in the presence of ADP and AMP-PNP as shown in Table 3). Binding was analyzed by fluorescence anisotropy as described in Experimental Procedures and plotted as a function of Mtr4p concentration. The curves overlaid on the data (—) represent the best fits of the data to the single-site binding model described by eq 5 or the cooperative binding model described by eq 6. Each datum represents the average of three independent measurements. Data were plotted as $\Delta A/\Delta A_{max}$ to best illustrate the differences in the data by providing the same lower and upper asymptotes of each curve. (B) Plots of the residual values for the curve fits in panel A (i.e., the difference between the calculated anisotropy from the curve fit and the experimental data) show no bias for data subsets, indicating a good fit to the model. (C) Representative binding isotherm for the association of Mtr4p with single-stranded 20, 10, and 5 nt random-sequence RNA in the absence of nucleotide. Binding was analyzed as described for panel A. (D) Plots of the residual values for the curve fits in panel C as described for panel B.

not cause a shift to single-site binding behavior for any of the nucleotide-bound states. This behavior agrees well with a calculated intersection site size of 5 nt (independent of nucleotide-bound status) as determined by MBDA. In the presence of AMP-PNP, the affinity of Mtr4p for A_{10} is weak, and we therefore cannot confidently distinguish between the single-site and modified Hill binding models. Despite the fact that approximately two binding sites remained for all nucleotide-bound states, we observed that the affinity of Mtr4p for A_{10} was lower for each of those states than that observed for A_{20}, most likely because of the loss of cooperative interactions that promote high-affinity binding. In the absence of nucleotide, a 2-fold decrease in affinity was observed. The addition of nucleotide caused a further decrease in affinity, approximately 3-fold in the presence of ADP and approximately 10-fold in the presence of AMP-PNP (Figure 2). Unlike the random-sequence substrate, because the site size of Mtr4p on poly(A) does not change significantly upon nucleotide binding, we can assess the contributions of losing binding sites and nucleotide binding to changes in affinity. It is clear that the loss of up to two binding sites on the poly(A) substrate decreases the affinity for that substrate (this change is similar in magnitude to that observed when R_{20} is truncated to R_{10} in the absence of nucleotide). In addition to the effect of removing binding sites, there appears to be an intrinsic loss of affinity induced by nucleotide binding that favors binding of Mtr4p to longer poly(A) tracts (i.e., the penalty for truncating from 20 to 10 adenylates is greater in both the ADP- and AMP-PNP-bound states than in the absence of nucleotide). This is similar to our previous observation

that a loss of affinity upon nucleotide binding can allow Mtr4p to discriminate 3′-tailed substrates from 5′-tailed substrates (*19*). Furthermore, because more than one binding site and thus the opportunity for cooperative interactions remain, binding of Mtr4p to the A_{10} substrate is tighter in all nucleotide-bound states than for the R_{10} substrate.

Truncation to 5 nt would leave at most a single binding site for any of the Mtr4p−substrate−nucleotide complexes. We observed that such truncation causes a significant decrease in affinity in the absence of nucleotide for both substrates. In the absence of nucleotide, the R_5 substrate contains a single binding site, resulting in an additional approximately 30-fold reduction in affinity relative to the R_{10} substrate (Figure 2). For the A_5 substrate in the absence of nucleotide, the presence of a single binding site results in an additional approximately 6-fold decrease in affinity relative to the A_{10} substrate and single-site binding behavior. Therefore, the poly(A) and random oligomer truncation studies are consistent with MBDA predictions for both substrates in the nucleotide-free complex. The presence of either ADP or AMP-PNP caused the affinity to decrease to $>2\ \mu$M for both the A_5 and R_5 substrates. It is intriguing that the binding site size of the Mtr4p−R_{20}−AMP-PNP complex is 17 nt, yet Mtr4p is able to bind the R_{10} and R_5 substrates. It is possible that Mtr4p binds R_{10} and R_5 in a mode that is distinct from that of R_{20} under certain conditions (i.e., nucleotide-bound, high protein concentration). Further, binding of Mtr4p to these shorter substrates is likely dependent on saturation binding, which occurs at high protein concentrations and might have less physiological relevance. These data indicate that a single binding site is a poorly interacting substrate. However, for a single binding site in the absence of bound nucleotide, a random-sequence substrate has a markedly lower baseline affinity than a poly(A) substrate.

These results show that as the number of binding sites available for Mtr4p to bind decreases, the affinity of Mtr4p for that substrate also decreases. In addition, because of the observed apparent cooperative behavior, Mtr4p binds to the 10 nt truncated poly(A) substrates with higher affinity than their random-sequence counterparts in all nucleotide-bound states. The loss of affinity upon truncation of the poly(A) substrates is exacerbated when either ADP or AMP-PNP is bound, whereas the effect of nucleotide binding to the truncated random-sequence substrates is less well-defined. This indicates that the mechanism by which Mtr4p is able to discriminate substrates derives from a combination of the number of available binding sites and the effect of nucleotide binding on both affinity and site size. Such a mechanism allows Mtr4p to effectively distinguish poly(A) from random substrates independent of its nucleotide-bound status.

The Mtr4p−Homopolymer Complex Is a Much Less Efficient ATPase Than the Complex with a Random-Sequence RNA. Efficient hydrolysis of ATP is a requirement for any helicase, and Mtr4p possesses RNA-dependent ATPase activity (*16*, *19*). The ability of Mtr4p to hydrolyze ATP in response to substrate-specific interactions is likely to have a significant impact on both substrate delivery and the efficiency of Mtr4p−exosome system-mediated processing. The ability of Mtr4p to hydrolyze ATP in the presence of the model substrates in Table 1 was assayed spectrophotometrically using a coupled enzyme assay. We found the sequence of the RNA substrate to have a profound effect on the Michaelis−Menten parameters of ATP hydrolysis. The Mtr4p−R_{20} complex is the most efficient ATPase. This is clear from the observed K_m (0.1 mM), k_{cat} (444 min^{-1}), and k_{max} (519 min^{-1}). Each of these parameters shows R_{20} to be at least 3-fold more efficient as a stimulator of Mtr4p ATPase activity than any other substrate tested (Figure 3 and Table 4). Unlike the other kinetic parameters, the K_{app}(RNA) for R_{20} (179 nM) is comparable to those of both the A_{20} (211 nM) and U_{20} (193 nM) substrates, indicating that affinity for the RNA substrate does not account for differences in catalytic rate. To ensure that the enzyme kinetic parameters determined were not significantly influenced by the experimental conditions, we determined the k_{cat} and K_m for the R_{20} substrate under physiological salt conditions, and at subsaturating RNA levels. Changing the buffer system to physiological salt had no effect on either k_{cat} or K_m (data not shown). At subsaturating RNA concentrations, the K_m was statistically indistinguishable ($p = 0.17$) from that under the saturated RNA conditions, and the k_{cat} was significantly reduced as expected (data not shown). The A_{20} and U_{20} substrates stimulate ATPase activity to a very similar degree. In fact, all of the kinetic parameters are statistically indistinguishable for the two substrates (Table 4). Despite the ability of Mtr4p to bind to $(UC)_{10}$, that substrate could not stimulate ATP hydrolysis. We observed measurable catalysis, but the rates determined were unreliable and very weak. For all of the substrates tested, the K_{app} values were significantly larger than the estimated affinity based on direct binding to the substrate in the presence of AMP-PNP (Table 3). These differences imply that the apparent binding constants include contributions from some other kinetically relevant event. The nature of the assay (i.e., substrate affinity is measured indirectly) precludes determination of which event is the source of this discrepancy.

Mtr4p, as part of its function in nuclear RNA processing, will encounter substrates truncated by the exosome. The manner in which Mtr4p responds to substrates that have been or are being truncated will in part determine which substrates can or cannot be processed. To examine the effect of substrate truncation on ATP hydrolysis, we determined the ATPase kinetic parameters for truncated random-sequence and poly(A) substrates. As we found in the binding affinity studies described above, RNA substrate truncation differentially affects Mtr4p ATP hydrolysis kinetics in the presence of random versus poly(A) substrates (Figure 3 and Table 4). Truncation of R_{20} to R_{10} decreases both the rates of ATP hydrolysis (k_{cat} and k_{max}, approximately 3-fold) and the affinity for both ATP and RNA (K_m and K_{app}, 6−10-fold). For the R_{20} and R_{10} substrates, $k_{cat} = k_{max}$, indicating that the same Mtr4p−ATP−RNA complex forms prior to catalysis, regardless of whether saturation is reached for the Mtr4p−ATP or Mtr4p−RNA complex (*46*). This is not the case for the R_5 substrate (below). In contrast, truncation of A_{20} to A_{10} had no effect on k_{cat} and k_{max}, but a severe effect on K_m (13-fold decrease) and K_{app} (2.4-fold decrease). Surprisingly, upon truncation of the R_{10} substrate to R_5, neither K_m nor K_{app} is appreciably affected, whereas k_{cat} and k_{max} are both decreased. Truncation of A_{10} to A_5 completely abolished the ability to stimulate Mtr4p ATP hydrolysis, despite the 10-fold higher affinity of A_5 relative to R_5 in the direct binding assay [in the absence of nucleotide (Table 3)]. This effect is probably due to a further decrease in the affinity of Mtr4p for ATP in the presence of the A_5 substrate. Because the K_m in the presence of A_{10} is 5.2 mM, any further decrease in affinity for ATP could conceivably abolish ATPase activity. These data indicate that decreasing the length of R_{20} can negatively impact both the apparent affinity for ATP and RNA and the chemical steps that facilitate ATP hydrolysis. In contrast, truncating a poly(A) substrate causes a loss of affinity for ATP and RNA, while the

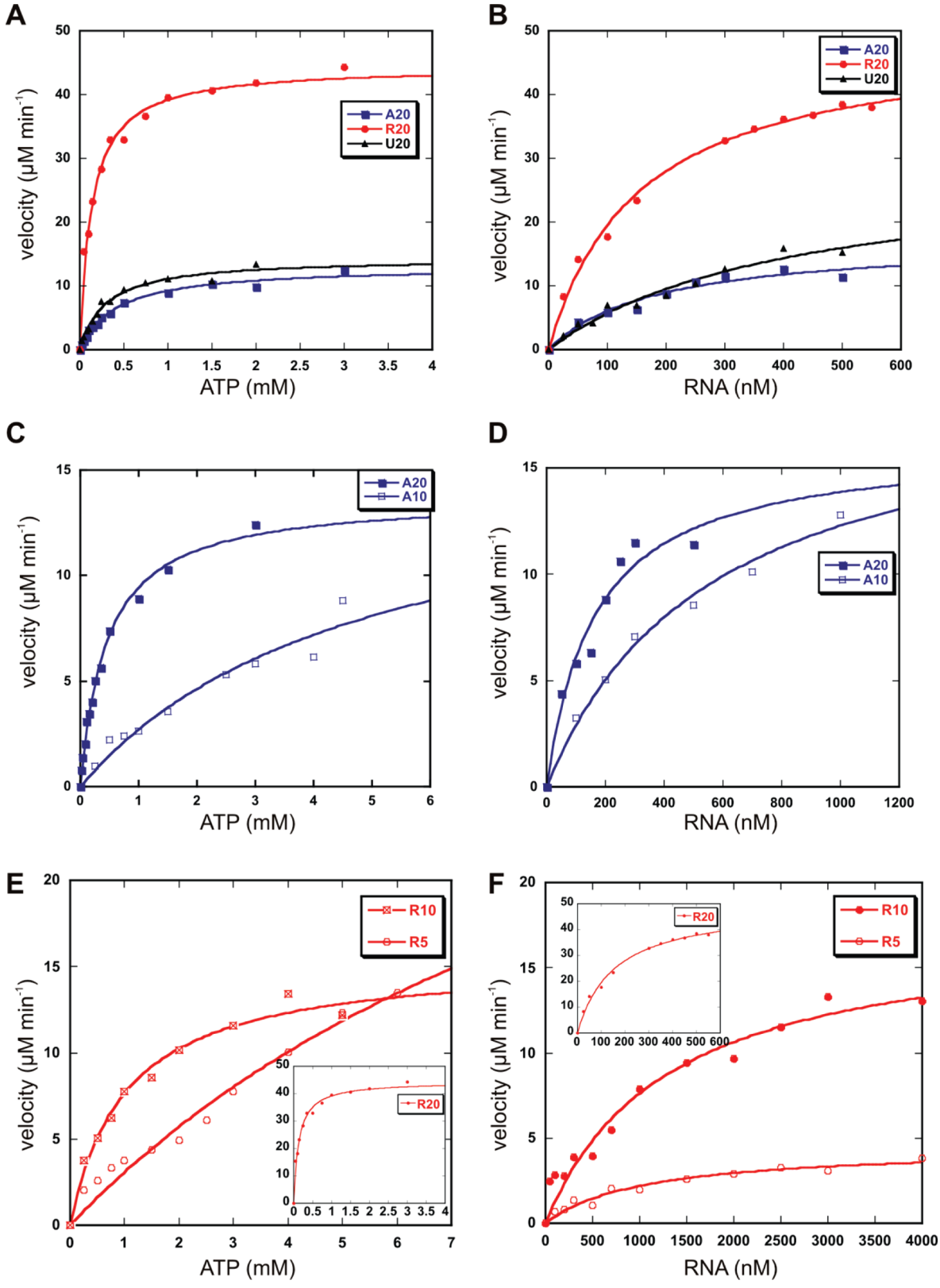

FIGURE 3: Michaelis−Menten kinetic parameters of Mtr4p ATPase activity are highly dependent on both substrate sequence and length. The ATPase activity of Mtr4p was measured using a spectrophotometric assay that couples ATP hydrolysis to the oxidation of NADH. The absorbance at 338 nm vs time measurements were used to determine initial rates (v) of ATP hydrolysis at each concentration of the variable component. Each experiment included fixed concentrations of Mtr4p (100 nM) and either ATP (4 mM) (A, C, and E) or RNA (500 nM A_{20}, R_{20}, R_{10}, A_{10}, and R_5 and 1 μM U_{20}) (B, D, and F). Plots of initial velocity vs substrate concentration were fit to the Michaelis−Menten equation using KaleidaGraph. Panels E and F show insets containing the R_{20} data to best illustrate the comparison between the shorter random substrates. The kinetic parameters derived from analysis of these experiments are listed in Table 4.

chemical processes involved in the hydrolysis of ATP are unaffected. In general, upon truncation of random-sequence substrates, Mtr4p has significantly higher affinity for ATP but weaker apparent affinity for RNA substrates. Importantly, a random-sequence

Table 5: Dissociation Kinetic Parameters of the Mtr4p−Substrate Interaction as a Function of Substrate and Nucleotide

substrate	nucleotide	k_1 (s^{-1})[a]	$t_{1/2}$-1 (s)[b]	k_2 (s^{-1})[c]	$t_{1/2}$-2 (s)[d]	%ΔA-1[e]	%ΔA-2[f]
A_{20}[g]	none[g]	0.015 ± 0.002	47.8 ± 7.8	0.0036 ± 0.0006	203.9 ± 31.8	39.2	60.8
A_{20}[g]	AMP-PNP[g]	0.032 ± 0.003	22.2 ± 2.4	0.010 ± 0.002	81.5 ± 25.6	75.4	24.6
A_{20}	ATP	0.046 ± 0.004	15.4 ± 1.3	not available	not available	not available	not available
R_{20}[g]	none[g]	0.039 ± 0.007	19.4 ± 4.4	not available	not available	not available	not available
R_{20}[g]	AMP-PNP[g]	0.077 ± 0.008	9.2 ± 1.0	0.0057 ± 0.002	145.7 ± 48.1	81.9	18.1
R_{20}	ATP	> 0.13	< 5	not available	not available	not available	not available
U_{20}	none	> 0.13	< 5	not available	not available	not available	not available
U_{20}	AMP-PNP	> 0.13	< 5	0.0036 ± 0.0003	193.7 ± 14.8	69.9	30.1
U_{20}	ATP	> 0.13	< 5	0.0029 ± 0.001	170.5 ± 33.9	17.8	82.2
$(UC)_{10}$	none	> 0.13	< 5	not available	not available	not available	not available
$(UC)_{10}$	AMP-PNP	> 0.13	< 5	not available	not available	not available	not available
$(UC)_{10}$	ATP	> 0.13	< 5	not available	not available	not available	not available

[a]Rate constant for the fast dissociation event. [b]Half-life for the fast dissociation event. [c]Rate constant for the slow dissociation event. [d]Half-life for the slow dissociation event. [e]Percent of anisotropy change associated with the fast dissociation event. [f]Percent of anisotropy change associated with the slow dissociation event. [g]Values are derived from previously reported experiments that have been re-evaluated (*19*).

substrate containing a maximum of one binding site can stimulate Mtr4p ATP hydrolysis, whereas a poly(A) substrate requires more than one binding site to stimulate Mtr4p ATP hydrolysis. Taken together, these data show that homopolymeric substrates attenuate the ATPase activity of Mtr4p relative to random-sequence substrates, most likely because of decreased affinity for ATP. These data further confirm that the interactions between random-sequence and poly(A) substrates are fundamentally distinct and therefore those substrates are likely to be processed differently by the Mtr4p−exosome system.

Homopolymeric Stretches Restrict Dissociation of the Mtr4p−RNA Complex. One potential role of Mtr4p is targeting substrates to the exosome. A natural requirement for targeting is that the Mtr4p−substrate complex remains intact. Therefore, substrates containing RNA sequence motifs that promote slowly dissociating Mtr4p−RNA complexes are more likely to be targeted to the exosome. Conversely, RNA substrates that contain sequence motifs that promote quickly dissociating Mtr4p−RNA complexes are likely to influence its catalytic cycle by promoting turnover of Mtr4p. The kinetics of dissociation describes the point at which hydrolysis of the Mtr4p−ATP complex promotes RNA structure modification through movement and/or enzyme recycling. Such recycling might be required for activity. The rate(s) of dissociation of an Mtr4p−RNA complex was determined by measuring the decrease in anisotropy as a function of time in the presence of the four 20 nt RNA sequences listed in Table 1. Unlabeled oligonucleotides are effective competitors for Mtr4p binding because the apparent inhibition constants ($K_{i,app}$) of each unlabeled oligonucleotide obtained via competition experiments were similar to measured affinities in direct binding experiments (ref *19* and data not shown). The decrease in anisotropy of the Mtr4p−RNA complex was analyzed using either a single-exponential or a double-exponential equation. The fits of the two model equations were compared using an *F*-test to determine the appropriate model. We took a p value of < 0.05 to indicate that the double-exponential equation provided a statistically significant improvement to the fit of the data. We have found that both substrate sequence and nucleotide binding can give rise to biphasic dissociation kinetics, yielding dissociation rates for a fast (k_1) and a slow (k_2) dissociating population. We first used this analysis to better describe the dissociation of the A_{20} and R_{20} substrates from Mtr4p, for which we had previously reported estimated half-lives based on a single-exponential fit (*19*) (indicated by the letter *g* in Table 5). The Mtr4p−R_{20} nucleotide-free complex has rapid but measurable dissociation kinetics and a single dissociating species with a rate of dissociation (k_1) of 0.046 s^{-1}, which corresponds to a half-life ($t_{1/2}$) of 15 s. Interestingly, the presence of AMP-PNP confers a second Mtr4p−R_{20} dissociating population ($p < 0.004$). The major population has a faster k_1 (0.077 s^{-1}; $t_{1/2} = 9$ s) than the nucleotide-free complex and encompasses approximately 82% of the total decrease in anisotropy (Figure 4). As the population of the second dissociating species contributes only 18% of the observed anisotropy decrease, the net result is a similar aggregate rate of dissociation to the nucleotide-free complex. The Mtr4p−A_{20} complex is much less dynamic and is characterized by the presence of at least two dissociating species both in the absence of nucleotide and in the AMP-PNP-bound complex. In the nucleotide-free Mtr4p−A_{20} complex, we detect two dissociating species, with the slower dissociating species ($k_2 = 0.0036$ s^{-1}; $t_{1/2} = 204$ s) contributing 61% to the overall decrease in anisotropy (Figure 4). We also detect two dissociating populations in the Mtr4p−A_{20}−AMP-PNP complex, but for that complex, both k_1 and k_2 are faster and k_1 dominates rather than k_2, yielding a faster overall rate of dissociation. This pattern does not appear to arise because of the homopolymeric nature of poly(A), as the Mtr4p−U_{20} complex dissociates very rapidly in its nucleotide-free form ($k_1 > 0.13$ s^{-1}; $t_{1/2} < 5$ s). The Mtr4p−U_{20}−AMP-PNP complex, like the equivalent R_{20} complex, contains a second, long-lived dissociating species. However, unlike the other complexes, AMP-PNP binding actually retards dissociation of the Mtr4p−U_{20}−AMP-PNP complex relative to that of the nucleotide-free form. The Mtr4p−$(UC)_{10}$ complex is extremely dynamic regardless of the presence of a nucleotide. The Mtr4p−$(UC)_{10}$ complex has a single dissociating species in all cases with a k of > 0.13 s^{-1} (Figure 4). For each substrate, we examined the rate of dissociation in the absence of nucleotide under physiological salt conditions to ensure that the ionic strength of our experimental conditions did not alter the trends we observed (data not shown).

We also examined dissociation kinetics in the presence of ATP. The conditions of this assay are nearly identical to those under which we conducted our ATPase assay, indicating that Mtr4p is hydrolyzing ATP during the course of the dissociation kinetics experiment. As expected, in the presence of ATP, the Mtr4p−R_{20} and Mtr4p−A_{20} complexes are much more dynamic and contain a single observable dissociating species, suggesting that ATP hydrolysis, and not just ATP binding, induces the release of the substrate (Table 5). However, under conditions of ATP

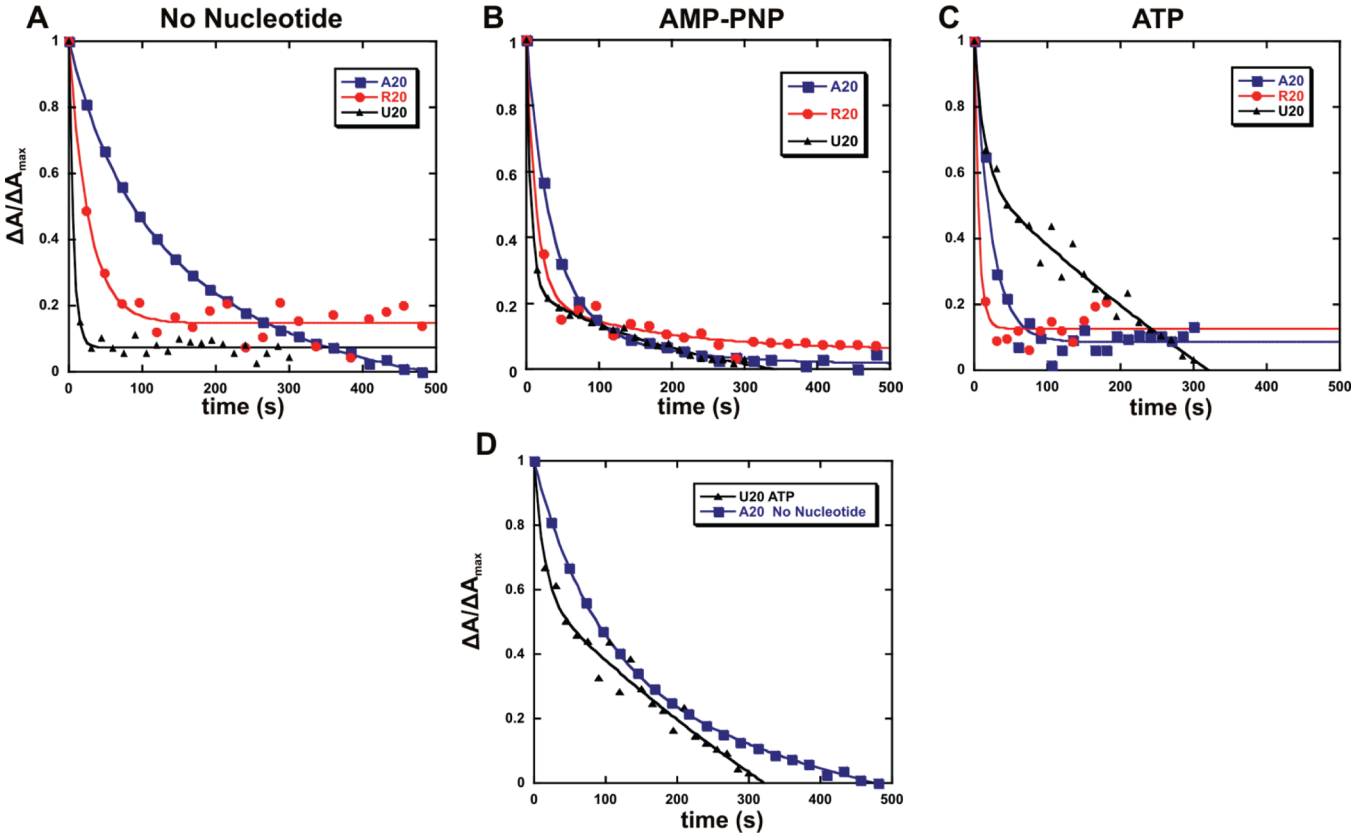

FIGURE 4: Homopolymeric substrates suppress Mtr4p complex dissociation. The Mtr4p−A_{20} complex is longer-lived than that of a complex between Mtr4p and either R_{20} or U_{20}. A preformed complex of Mtr4p and either Fl-A_{20}, Fl-R_{20}, or Fl-U_{20} (Table 1) was challenged with a 5000-fold molar excess of unlabeled RNA of the same sequence and the anisotropy measured as a function of time. Each datum represents the mean value of triplicate measurements. The rate of dissociation (k) of each complex was determined by fitting the anisotropy vs time curves to either a single-exponential or a double-exponential equation. Details of dissociating kinetic parameters derived from this analysis are listed in Table 5. Dissociation kinetic curves of the (A) Mtr4p−RNA complexes in the absence of nucleotide, (B) Mtr4p−RNA−AMP-PNP complexes, and (C) Mtr4p−RNA−ATP complexes. (D) Comparison of the dissociation kinetics of the Mtr4p−A_{20} and Mtr4p−U_{20}−ATP complexes showing that the Mtr4p−A_{20}−no nucleotide complex has the least dynamic interaction.

hydrolysis, the dissociation rate of the R_{20} complex (k_1 > 0.13 s^{-1}; $t_{1/2}$ < 5 s) is significantly faster than that of the A_{20} complex (k_1 = 0.046 s^{-1}; $t_{1/2}$ = 15 s). Strikingly, the formation of the Mtr4p−U_{20}−ATP complex severely retards complex dissociation. Further, the Mtr4p−U_{20}−ATP and Mtr4p−U_{20}−AMP-PNP complexes contain two dissociating species with nearly equal rates of dissociation but for which the amount that each species contributes to the overall rate of dissociation is markedly different for ATP and AMP-PNP. In the presence of AMP-PNP, nearly 70% of the population is in the faster dissociating species (k_1 > 0.13 s^{-1}; $t_{1/2}$ < 5 s). The Mtr4p−U_{20}−ATP complex favors the k_2 state (0.0029 s^{-1}; $t_{1/2}$ = 171 s; this population encompasses approximately 82% of the total decrease in the anisotropy amplitude). Thus, both ATP binding and to a much greater extent ATP hydrolysis inhibit the dissociation of Mtr4p from poly(U) substrates, whereas ATP hydrolysis clearly accelerates dissociation from the R_{20} and A_{20} substrates. On the basis of these data, we conclude that each of the Mtr4p−RNA complexes (with and without nucleotide) studied here has unique, sequence-specific interactions with Mtr4p, which generates a particular dissociation kinetic profile for each species. Most importantly, there must be a distinct interaction with poly(A) that slows Mtr4p dissociation relative to the random-sequence substrate in a manner independent of nucleotide binding or hydrolysis.

DISCUSSION

The mechanism whereby Mtr4p interacts with its substrates has a great impact on all its functions: helicase activity, ATPase activity, and the putative targeting function. All three of these functions are no doubt intimately related as part of the coordination of Mtr4p activity with degradation by the exonucleolytic exosome complex. While both the addition of short 3′-poly(A) tails and the degradation of substrates containing those tails have been well documented, the pathway from polyadenylation to eventual degradation remains undefined. Polyadenylation is an energetic investment the cell makes to ensure timely degradation or processing of a given substrate. One way to guarantee that the investment will produce the desired outcome is to directly target the polyadenylated substrate to the degradation machinery. There is precedent for such targeting in RNA processing. Mammalian AU-rich element (ARE) binding proteins direct substrates to the cytoplasmic exosome for exonucleolytic decay (*47*). Likewise, the *Schizosaccharomyces pombe* poly(A)-binding protein 2 (Pab2) can target some polyadenylated snoRNAs to the *S. pombe* exosome (*48*). For targeting to occur, the protein−RNA complex formed must possess properties that make encounters with the degradation machinery more likely. The data we report here show that *S. cerevisiae* Mtr4p, which is both a poly(A)-binding protein like *S. pombe* Pab2 and a helicase, forms a complex with poly(A) RNA that is ideally suited for targeting to the exosome. In particular, the Mtr4p−poly(A)

complex promotes cooperative interactions that drive high-affinity binding, is comparatively resistant to truncation, and possesses an attenuated propensity to dissociate in response to either competing RNA substrates or ATP hydrolysis. Many substrates encountered by Mtr4p in vivo will be of mixed sequence, with stretches of poly(A) and random or U-rich regions. On the basis of our data, it is likely that the behavior of such a complex will depend on the length of the poly(A) tract and the length of the sequence located to the 5′ side of the poly(A) tract. We anticipate that a substrate with more than 10 adenylates at the 3′-end will behave largely like the poly(A) model substrate described here. As a caveat, an A-rich region within the interior of a substrate may exhibit different behavior than that observed for a poly(A) 3′-end. It is also possible that an extended (i.e., 10−20 or more adenylates) poly(A) tract at the 3′-end of a substrate could form a complex in which Mtr4p proteins bound to the poly(A) region tether another Mtr4p protein (or proteins) to a 5′-stretch of random sequence adjacent to, e.g., an element of secondary structure.

On the basis of the MBDA analysis, one can distill the poly(A) and random substrates down to a minimal site of ≈5 nt. In agreement with our results, a recent crystal structure of an Mtr4p−A_{10}−ADP complex (*22*) confirms that in its main interaction mode with poly(A) Mtr4p contacts 5 nt. For that minimal site, Mtr4p binds poly(A) approximately 10-fold more tightly than the random-sequence substrate. Thus, at any given time, there will be many more Mtr4p−short poly(A) complexes than similar complexes with random-sequence substrates, thereby increasing the likelihood of Mtr4p−poly(A) complexes encountering other RNA processing factors. Such a property could play an important role in promoting multiple rounds of polyadenylation and degradation, which might be required for highly structured substrates (*12*). For example, given the preference of Mtr4p for poly(A), the frequency of delivery of a substrate to the Trf/Air polyadenylation complexes should increase if, for example, the substrate has already undergone limited polyadenylation and/or partial degradation. Because most of the Mtr4p present in the cell exists outside the TRAMP complex (*11*), one role of Mtr4p could be to recruit the Trf/Air polyadenylation complexes to partially adenylated substrates to ensure the creation of a footprint sufficient to foster degradation by the exosome. Nucleotide binding markedly decreases the affinity of Mtr4p for the A_5 substrate, suggesting that ATP binding can be an effective regulator of poly(A) selection. As the number of binding sites increases, the differences in affinity between the poly(A) and random-sequence substrates [and the poly(U) and poly(UC) substrates] become smaller; however, Mtr4p can still discriminate RNA substrates because other characteristics of the complexes still differ markedly. The basis for discrimination most likely lies in the large differences in the architecture of the Mtr4p−poly(A) complexes relative to the complexes with random-sequence substrates, and changes in the architecture of the Mtr4p−poly(A) complexes in response to nucleotide binding and hydrolysis. Comparison of the apo and Mtr4p−A_{10}−ADP structures shows significant structural shifts, particularly in domains 2 and 4, which contact the bound RNA (not shown). These shifts are consistent with the Mtr4p−ssRNA complex architectural changes suggested by our MBDA analysis. While it is possible that the KOW domain of Mtr4p stabilizes some substrate complexes, all available data suggest that this happens at high protein concentrations (*22*), far beyond that required to saturate Mtr4p binding with our model substrates. Moreover, while it is likely that the KOW domain may contribute to binding some substrates, other contacts appear to make more important contributions to binding affinity. In particular, the 3′-end of the A_{10} substrate in the cocrystal abuts the interface between domains 1 and 4, with interactions between R272 and O4′ of the 3′-ribose and between R1030 and the exocyclic amino group of the 3′-adenosine. Adjacent to the 5′-most observed nucleotide, there is a large solvent channel that could easily accommodate the remainder of the A_{10} substrate. Despite the proximity of the KOW domain to the region where the 5′-end of the A_{10} substrate likely resides, no contacts between the two are evident. However, with larger substrates, or perhaps in different nucleotide-bound states, the KOW domain could, either by the nature of this proximity or by nucleotide-induced conformational rearrangement, productively interact with a bound RNA substrate.

Our studies of the kinetics of ATP hydrolysis and dissociation of the Mtr4p−RNA complex show suppression of both activity and complex dissolution consistent with the putative targeting function. The efficiency of targeting a given substrate to the exosome machinery will depend in part on how long that substrate stays bound to the protein that does the targeting. In turn, nucleotide binding and hydrolysis can have a strong effect on the stability of the Mtr4p−RNA complex. We observe that the homopolymeric A_{20} and U_{20} substrates are much less efficient stimulators of Mtr4p ATP hydrolysis than the R_{20} substrate (Table 4). The difference in efficiency is particularly striking for the single-binding site (A_5 and R_5) substrates. The R_5 substrate can stimulate Mtr4p ATPase activity, with a catalytic rate ($101 \pm 5\ min^{-1}$) that is statistically indistinguishable from that of the A_{20} substrate [$124 \pm 18\ min^{-1}$; however, the affinities for both ATP and RNA are far weaker for the R_5 substrate than the A_{20} substrate (see Table 4)]. These differences in ATPase activity are not likely due to effects of RNA secondary structure. While the R_{20} substrate might form transient secondary structures during the time course of our experiment, the R_5 substrate most certainly cannot form such structures. Therefore, the attenuated ATPase activity observed for the A_{20} and U_{20} substrates arises because of a fundamental difference in the way Mtr4p interacts with these substrates relative to the random-sequence substrate. Furthermore, the steady-state cellular ATP concentration in yeast is approximately 4−8 mM (*49*) and can vary significantly depending on growth conditions (*50*). If the nuclear/nucleolar concentration of free ATP falls within the same range and the RNA substrate concentration is saturating, then we would expect the response of Mtr4p−substrate complexes in vivo to ATP to vary considerably with substrate sequence. In particular, for complexes with random-sequence 3′-tails as short as 5 nt, Mtr4p should be able to hydrolyze ATP with at least moderate efficiency because ATP is likely to be saturating for those complexes. In contrast, this amount of ATP will likely be subsaturating for a poly(A) tail as long as 10 nt, and therefore, ATP hydrolysis is expected to be comparatively inefficient. In conjunction with suppressed ATPase activity, we observe a marked decrease in the rate of dissociation for the A_{20} substrate relative to the R_{20} substrate. When compared with the other substrates, the Mtr4p−A_{20} complex is the least dynamic (Figure 4D). These data suggest that, in the absence of nucleotide, poly(A)-tailed substrates would dissociate slowly, allowing the RNA to be targeted to the exosome. The presence of AMP-PNP increases the dynamics of both the Mtr4p−A_{20} and Mtr4p−R_{20} complexes relative to the absence of nucleotide. In the presence of ATP, the Mtr4p−A_{20} and Mtr4p−R_{20} complexes are much more dynamic, suggesting

that ATP hydrolysis, and not just ATP binding, induces the release of the substrate (Table 5). However, in the presence of ATP, release of the substrate is still markedly slower for the A_{20} substrate than for the R_{20} substrate. These data show that, regardless of the nucleotide-bound state, the Mtr4p−poly(A) substrate complex is less likely to dissociate than the Mtr4p complex with a random-sequence substrate, thus providing a greater window of opportunity for Mtr4p to deliver the poly(A) substrate to the exosome. Further, the rate of dissociation of the Mtr4p−R_{20}−ATP complex indicates that Mtr4p, absent a functional tether (e.g., the exosome), will rapidly release a random-sequence substrate upon hydrolysis of ATP.

Curiously, the Mtr4p−U_{20} complexes exhibit the opposite trend in dissociation kinetics relative to Mtr4p−A_{20} complexes. The Mtr4p−U_{20} association is highly dynamic in the absence of nucleotide ($t_{1/2} < 5$ s). Upon binding AMP-PNP, the complex becomes less dynamic. The Mtr4p−U_{20}−ATP complex is the least dynamic complex of the three. Under our experimental conditions, active ATP hydrolysis should proceed during the dissociation kinetics experiment. This suggests that ATP hydrolysis impedes dissociation. The significance of this observation is unknown, but it is possible that under certain circumstances Mtr4p might be able to target U-rich substrates to the Trf/Air polyadenylation complexes or the exosome.

In addition to substrate targeting, the rate of complex dissociation as a function of nucleotide binding and hydrolysis is likely to have an impact on both ATPase and RNA structure remodeling activities of Mtr4p. For the DEAD-box helicases, a study in which progression through the ATP hydrolysis cycle was blocked via the use of nonhydrolyzable analogues showed that one function of ATP hydrolysis is to allow enzyme recycling and multiple substrate turnovers that enhance the rate of unwinding (*51*). Most importantly, the authors demonstrated that ATP hydrolysis stimulates enzyme dissociation as part of the recycling process. Because we also observe that the rate of dissociation for both the A_{20} and R_{20} substrates increases significantly in the presence of ATP (Figure 4), it is likely that such rapid substrate release is an integral feature of the catalytic activity of Mtr4p. In fact, the R_{20} substrate exhibits both the most rapid dissociation kinetics in the presence of ATP and the most robust stimulation of Mtr4p ATPase activity.

In summary, we view targeting as a stochastic process that reflects the increased likelihood that a given protein−RNA complex will encounter the degradation machinery. Each of the unique features of the Mtr4p−poly(A) complex that we observe (i.e., increased affinity, suppressed ATP hydrolysis, and decreased rate of dissociation) stems from the unique binding mechanism used by Mtr4p to interact with poly(A). Each feature alone could increase the likelihood that an Mtr4p−poly(A) complex will encounter RNA processing factors relative to other substrates. Together, these features are likely to markedly increase the efficiency with which polyadenylated substrates are targeted to either the polyadenylation or degradation machinery.

ACKNOWLEDGMENT

We thank Dr. Laura Mizoue of the Center for Structural Biology at Vanderbilt University (Nashville, TN) for providing the expression plasmid used in these studies. We also acknowledge the assistance of Paz J. Luncsford with several control experiments.

REFERENCES

1. Butler, J. S. (2002) The yin and yang of the exosome. *Trends Cell Biol. 12*, 90–96.
2. Dziembowski, A., Lorentzen, E., Conti, E., and Seraphin, B. (2007) A single subunit, Dis3, is essentially responsible for yeast exosome core activity. *Nat. Struct. Mol. Biol. 14*, 15–22.
3. Lorentzen, E., Basquin, J., and Conti, E. (2008) Structural organization of the RNA-degrading exosome. *Curr. Opin. Struct. Biol. 18*, 709–713.
4. Mitchell, P., Petfalski, E., Shevchenko, A., Mann, M., and Tollervey, D. (1997) The exosome: A conserved eukaryotic RNA processing complex containing multiple 3′→ 5′ exoribonucleases. *Cell 91*, 457–466.
5. Burkard, K. T., and Butler, J. S. (2000) A nuclear 3′-5′ exonuclease involved in mRNA degradation interacts with poly(A) polymerase and the hnRNA protein Npl3p. *Mol. Cell. Biol. 20*, 604–616.
6. Callahan, K. P., and Butler, J. S. (2008) Evidence for core exosome independent function of the nuclear exoribonuclease Rrp6p. *Nucleic Acids Res. 36*, 6645–6655.
7. Allmang, C., Kufel, J., Chanfreau, G., Mitchell, P., Petfalski, E., and Tollervey, D. (1999) Functions of the exosome in rRNA, snoRNA and snRNA synthesis. *EMBO J. 18*, 5399–5410.
8. van Hoof, A., Lennertz, P., and Parker, R. (2000) Yeast exosome mutants accumulate 3′-extended polyadenylated forms of U4 small nuclear RNA and small nucleolar RNAs. *Mol. Cell. Biol. 20*, 441–452.
9. Bird, G., Fong, N., Gatlin, J. C., Farabaugh, S., and Bentley, D. L. (2005) Ribozyme cleavage reveals connections between mRNA release from the site of transcription and pre-mRNA processing. *Mol. Cell 20*, 747–758.
10. Torchet, C., Bousquet-Antonelli, C., Milligan, L., Thompson, E., Kufel, J., and Tollervey, D. (2002) Processing of 3′-extended read-through transcripts by the exosome can generate functional mRNAs. *Mol. Cell 9*, 1285–1296.
11. LaCava, J., Houseley, J., Saveanu, C., Petfalski, E., Thompson, E., Jacquier, A., and Tollervey, D. (2005) RNA degradation by the exosome is promoted by a nuclear polyadenylation complex. *Cell 121*, 713–724.
12. Vanacova, S., Wolf, J., Martin, G., Blank, D., Dettwiler, S., Friedlein, A., Langen, H., Keith, G., and Keller, W. (2005) A new yeast poly(A) polymerase complex involved in RNA quality control. *PLoS Biol. 3*, e189.
13. Carneiro, T., Carvalho, C., Braga, J., Rino, J., Milligan, L., Tollervey, D., and Carmo-Fonseca, M. (2008) Inactivation of cleavage factor I components Rna14p and Rna15p induces sequestration of small nucleolar ribonucleoproteins at discrete sites in the nucleus. *Mol. Biol. Cell 19*, 1499–1508.
14. Schmid, M., and Jensen, T. H. (2008) Quality control of mRNP in the nucleus. *Chromosoma 117*, 419–429.
15. Kadaba, S., Wang, X., and Anderson, J. T. (2006) Nuclear RNA surveillance in *Saccharomyces cerevisiae*: Trf4p-dependent polyadenylation of nascent hypomethylated tRNA and an aberrant form of 5S rRNA. *RNA 12*, 508–521.
16. Wang, X., Jia, H., Jankowsky, E., and Anderson, J. T. (2008) Degradation of hypomodified tRNA(iMet) in vivo involves RNA-dependent ATPase activity of the DExH helicase Mtr4p. *RNA 14*, 107–116.
17. Thiebaut, M., Kisseleva-Romanova, E., Rougemaille, M., Boulay, J., and Libri, D. (2006) Transcription termination and nuclear degradation of cryptic unstable transcripts: A role for the nrd1-nab3 pathway in genome surveillance. *Mol. Cell 23*, 853–864.
18. Wyers, F., Rougemaille, M., Badis, G., Rousselle, J. C., Dufour, M. E., Boulay, J., Regnault, B., Devaux, F., Namane, A., Seraphin, B., Libri, D., and Jacquier, A. (2005) Cryptic pol II transcripts are degraded by a nuclear quality control pathway involving a new poly(A) polymerase. *Cell 121*, 725–737.
19. Bernstein, J., Patterson, D. N., Wilson, G. M., and Toth, E. A. (2008) Characterization of the essential activities of *Saccharomyces cerevisiae* Mtr4p, a 3′→5′ helicase partner of the nuclear exosome. *J. Biol. Chem. 283*, 4930–4942.
20. Bernstein, K. A., Granneman, S., Lee, A. V., Manickam, S., and Baserga, S. J. (2006) Comprehensive mutational analysis of yeast DEXD/H box RNA helicases involved in large ribosomal subunit biogenesis. *Mol. Cell. Biol. 26*, 1195–1208.
21. Jackson, R. N., Klauer, A. A., Hintze, B. J., Robinson, H., van Hoof, A., and Johnson, S. J. (2010) The crystal structure of Mtr4 reveals a novel arch domain required for rRNA processing. *EMBO J. 29*, 2205–2216.
22. Weir, J. R., Bonneau, F., Hentschel, J., and Conti, E. (2010) Structural analysis reveals the characteristic features of Mtr4, a DExH helicase

involved in nuclear RNA processing and surveillance. *Proc. Natl. Acad. Sci. U.S.A. 107*, 12139–12144.
23. Buttner, K., Nehring, S., and Hopfner, K. P. (2007) Structural basis for DNA duplex separation by a superfamily-2 helicase. *Nat. Struct. Mol. Biol. 14*, 647–652.
24. de la Cruz, J., Kressler, D., Tollervey, D., and Linder, P. (1998) Dob1p (Mtr4p) is a putative ATP-dependent RNA helicase required for the 3′ end formation of 5.8S rRNA in *Saccharomyces cerevisiae*. *EMBO J. 17*, 1128–1140.
25. Wilson, G. M., Sutphen, K., Moutafis, M., Sinha, S., and Brewer, G. (2001) Structural remodeling of an A + U-rich RNA element by cation or AUF1 binding. *J. Biol. Chem. 276*, 38400–38409.
26. Brahms, J., Michelson, A. M., and Van Holde, K. E. (1966) Adenylate oligomers in single- and double-strand conformation. *J. Mol. Biol. 15*, 467–488.
27. Deo, R. C., Bonanno, J. B., Sonenberg, N., and Burley, S. K. (1999) Recognition of polyadenylate RNA by the poly(A)-binding protein. *Cell 98*, 835–845.
28. Link, T. M., Valentin-Hansen, P., and Brennan, R. G. (2009) Structure of *Escherichia coli* Hfq bound to polyriboadenylate RNA. *Proc. Natl. Acad. Sci. U.S.A. 106*, 19292–19297.
29. Hofacker, I. L. (2003) Vienna RNA secondary structure server. *Nucleic Acids Res. 31*, 3429–3431.
30. Zuker, M. (2003) Mfold web server for nucleic acid folding and hybridization prediction. *Nucleic Acids Res. 31*, 3406–3415.
31. Young, P. R., and Kallenbach, N. R. (1978) Secondary structure in polyuridylic acid. Non-classical hydrogen bonding and the function of the ribose 2′-hydroxyl group. *J. Mol. Biol. 126*, 467–479.
32. Bujalowski, W. (2006) Thermodynamic and kinetic methods of analyses of protein-nucleic acid interactions. From simpler to more complex systems. *Chem. Rev. 106*, 556–606.
33. Bujalowski, W., and Jezewska, M. J. (1995) Interactions of *Escherichia coli* primary replicative helicase DnaB protein with single-stranded DNA. The nucleic acid does not wrap around the protein hexamer. *Biochemistry 34*, 8513–8519.
34. Deckman, I. C., and Draper, D. E. (1985) Specific interaction between ribosomal protein S4 and the α operon messenger RNA. *Biochemistry 24*, 7860–7865.
35. Gotoh, H., Kajikawa, M., Kato, H., and Suto, K. (1999) Intracellular Mg^{2+} surge follows Ca^{2+} increase during depolarization in cultured neurons. *Brain Res. 828*, 163–168.
36. Kao-Huang, Y., Revzin, A., Butler, A. P., O'Conner, P., Noble, D. W., and von Hippel, P. H. (1977) Nonspecific DNA binding of genome-regulating proteins as a biological control mechanism: Measurement of DNA-bound *Escherichia coli* lac repressor in vivo. *Proc. Natl. Acad. Sci. U.S.A. 74*, 4228–4232.
37. Kato, H., Gotoh, H., Kajikawa, M., and Suto, K. (1998) Depolarization triggers intracellular magnesium surge in cultured dorsal root ganglion neurons. *Brain Res. 779*, 329–333.
38. Jezewska, M. J., and Bujalowski, W. (1996) A general method of analysis of ligand binding to competing macromolecules using the spectroscopic signal originating from a reference macromolecule. Application to *Escherichia coli* replicative helicase DnaB protein nucleic acid interactions. *Biochemistry 35*, 2117–2128.
39. Wilson, G. M., Sun, Y., Lu, H., and Brewer, G. (1999) Assembly of AUF1 oligomers on U-rich RNA targets by sequential dimer association. *J. Biol. Chem. 274*, 33374–33381.
40. Dandliker, W. B., Hsu, M. L., Levin, J., and Rao, B. R. (1981) Equilibrium and kinetic inhibition assays based upon fluorescence polarization. *Methods Enzymol. 74*, 3–28.
41. Lundblad, J. R., Laurance, M., and Goodman, R. H. (1996) Fluorescence polarization analysis of protein-DNA and protein-protein interactions. *Mol. Endocrinol. 10*, 607–612.
42. Wilson, G. M. (2005) RNA Folding and RNA-Protein Binding Analyzed by Fluorescence Anisotropy and Resonance Energy Transfer. In Reviews in Fluorescence (Geddes, C. D., and Lakowicz, J. R., Eds.) pp 223−243, Springer Science and Business Media, Inc., New York.
43. Heilman-Miller, S. L., Thirumalai, D., and Woodson, S. A. (2001) Role of counterion condensation in folding of the *Tetrahymena* ribozyme. I. Equilibrium stabilization by cations. *J. Mol. Biol. 306*, 1157–1166.
44. Seifried, S. E., Wang, Y., and von Hippel, P. H. (1988) Fluorescent modification of the cysteine 202 residue of *Escherichia coli* transcription termination factor ρ. *J. Biol. Chem. 263*, 13511–13514.
45. Jezewska, M. J., Rajendran, S., and Bujalowski, W. (1998) Transition between different binding modes in rat DNA polymerase β-ssDNA complexes. *J. Mol. Biol. 284*, 1113–1131.
46. Tsu, C. A., and Uhlenbeck, O. C. (1998) Kinetic analysis of the RNA-dependent adenosinetriphosphatase activity of DbpA, an *Escherichia coli* DEAD protein specific for 23S ribosomal RNA. *Biochemistry 37*, 16989–16996.
47. Chen, C. Y., Gherzi, R., Ong, S. E., Chan, E. L., Raijmakers, R., Pruijn, G. J., Stoecklin, G., Moroni, C., Mann, M., and Karin, M. (2001) AU binding proteins recruit the exosome to degrade ARE-containing mRNAs. *Cell 107*, 451–464.
48. Lemay, J. F., D'Amours, A., Lemieux, C., Lackner, D. H., St-Sauveur, V. G., Bahler, J., and Bachand, F. (2010) The nuclear poly(A)-binding protein interacts with the exosome to promote synthesis of noncoding small nucleolar RNAs. *Mol. Cell 37*, 34–45.
49. Theobald, U., Mailinger, W., Baltes, M., Rizzi, M., and Reuss, M. (1997) In vivo analysis of metabolic dynamics in *Saccharomyces cerevisiae*: I. Experimental observations. *Biotechnol. Bioeng. 55*, 305–316.
50. Thomsson, E., Gustafsson, L., and Larsson, C. (2005) Starvation response of *Saccharomyces cerevisiae* grown in anaerobic nitrogen- or carbon-limited chemostat cultures. *Appl. Environ. Microbiol. 71*, 3007–3013.
51. Liu, F., Putnam, A., and Jankowsky, E. (2008) ATP hydrolysis is required for DEAD-box protein recycling but not for duplex unwinding. *Proc. Natl. Acad. Sci. U.S.A. 105*, 20209–20214.